scientific reports

Check for updates

OPEN

Translational approach for dementia subtype classification using convolutional neural network based on EEG connectome dynamics

Thawirasm Jungrungrueang[1], Sawrawit Chairat[1], Kasidach Rasitanon[2], Praopim Limsakul[2] & Krit Charupanit[1]✉

Dementia spectrum disorders, characterized by progressive cognitive decline, pose a significant global health burden. Early screening and diagnosis are essential for timely and accurate treatment, improving patient outcomes and quality of life. This study investigated dynamic features of resting-state electroencephalography (EEG) functional connectivity to identify characteristic patterns of dementia subtypes, such as Alzheimer's disease (AD) and frontotemporal dementia (FD), and to evaluate their potential as biomarkers. We extracted distinctive statistical features, including mean, variance, skewness, and Shannon entropy, from brain connectivity measures, revealing common alterations in dementia, specifically a generalized disruption of Alpha-band connectivity. Distinctive characteristics were found, including generalized Delta-band hyperconnectivity with increased complexity in AD and disrupted phase-based connectivity in Theta, Beta, and Gamma bands for FD. We also employed a convolutional neural network model, enhanced with these dynamic features, to differentiate between dementia subtypes. Our classification models achieved a multiclass classification accuracy of 93.6% across AD, FD, and healthy control groups. Furthermore, the model demonstrated 97.8% and 96.7% accuracy in differentiating AD and FD from healthy controls, respectively, and 97.4% accuracy in classifying AD and FD in pairwise classification. These establish a high-performance deep learning framework utilizing dynamic EEG connectivity patterns as potential biomarkers, offering a promising approach for early screening and diagnosis of dementia spectrum disorders using EEG. Our findings suggest that analyzing brain connectivity dynamics as a network and during cognitive tasks could offer more valuable information for diagnosis, assessing disease severity, and potentially identifying personalized neurological deficits.

Keywords Alzheimer's disease, Frontotemporal dementia, Electroencephalogram, Convolutional neural network, Aging disorders, Brain connectivity

Dementia spectrum disorders are a group of neurodegenerative diseases characterized by a progressive decline in cognitive functions of the brain that affect memory, language, planning, and behavior[1]. These disorders, such as Alzheimer's disease (AD) and frontotemporal dementia (FD), significantly impact both individuals and their caregivers in mental and economic aspects[2,3]. With a global population of approximately 55 million people living with dementia as of 2022, this number is projected to rise as populations age, making dementia a pressing public health concern[4]. Despite the increasing prevalence of dementia, early diagnosis and timely treatment of dementia remain challenging, as initial symptoms are often subtle and can easily be mistaken for other neurological conditions[5].

Although neuroimaging techniques such as computed tomography and magnetic resonance imaging (MRI) can aid in diagnosing dementia, their high cost and accessibility limitations may restrict widespread use[6]. Electroencephalography (EEG), a non-invasive method that records brain electrical activity, offers a more

[1]Department of Biomedical Sciences and Biomedical Engineering, Faculty of Medicine, Prince of Songkla University, Songkhla, Thailand. [2]Division of Physical Science, Faculty of Science, Prince of Songkla University, Songkhla, Thailand. ✉email: krit.ch@psu.ac.th

affordable and accessible alternative. Due to its cost-effectiveness and availability, EEG is well suited for large-scale screening and early detection of dementia. However, traditional interpretation of EEG data typically requires specialized expertise and can be time-consuming and subjective[7,8].

Recent advancements in machine learning algorithms, especially deep learning models, have significantly enhanced the diagnostic potential of EEG, transforming it into a powerful tool for detecting various neurological states and disorders, such as sleep stage scoring[9], seizure prediction in epilepsy[9,10], Parkinson's disease[11], schizophrenia[12], and dementia[13]. Machine learning algorithms not only automate the processing of complex EEG data, making the process faster and more flexible, but also enhance traditional feature-engineering methods with their capability to extract meaningful features from minimally preprocessed EEG data[9].

Researchers have demonstrated the effectiveness of machine learning algorithms in distinguishing individuals with dementia using EEG features. By using decision trees and random forests, time-domain statistics and frequency band energy were utilized to achieve classification accuracies of 78.5% and 86.3%, respectively, in detecting AD and FD from healthy control (HC)[14]. Utilizing maximal overlap discrete wavelets transform coefficients and linear discriminant analysis, reported a 93.18% accuracy in differentiating AD patients from HC[15] while employing phase locking value with a multiplex network-based approach, which analyzes the functional integration and segregation of brain networks, was shown to classify AD from HC with 92.5% accuracy[16]. Functional connectivity features with gradient boosting machines reported accuracy of 98.3% and 97.5% in AD and behavioral-variant FD from HC, respectively[17]. Recently, deep learning algorithms, such as convolutional neural networks (CNN), have also been successfully applied to multiclass classification (AD, FD, and HC) with an accuracy of up to 92.5% based on EEG functional connectivity[13]. These findings emphasize the potential of deep learning approaches for dementia subtype diagnosis.

Despite the promising application of EEG with machine learning in dementia diagnosis, a knowledge gap remains in understanding the dynamic patterns of brain connectivity, as previous studies have relied mainly on static features, such as instantaneous or mean connectivity. This study aims to analyze the dynamic brain connectivity profiles associated with dementia subtypes. We hypothesize that dementia subtypes exhibit distinct changes in brain connectivity dynamics, which could enhance our understanding of the bioelectrical alterations in dementia and potentially serve as novel biomarkers. Furthermore, we apply these dynamic connectivity profiles in our proposed CNN model for dementia subtype classification. We propose that a deep learning model incorporating dynamic connectivity features could improve their performance in dementia subtype diagnosis compared to the model using static features. This approach could facilitate early diagnosis, provide insights into neural mechanisms, and establish a novel framework for targeted interventions. Ultimately, our model could potentially be implemented as a fully automated diagnostic tool in clinical practice, contributing to more effective dementia management.

Results

Distinctive connectivity profiles of dementia subtypes

The distinctive connectivity profiles associated with dementia subtypes were revealed through a comprehensive analysis of dynamic features (e.g., mean, variance, skewness, and Shannon entropy) of brain connectivity measures, including inter-site phase clustering (ISPC), weighted phase lag index (wPLI), and amplitude envelope correlation (AEC) in five frequency bands (Delta, Theta, Alpha, Beta, and Gamma) (Fig. 1). The ISPC and wPLI measure indicates the correlation in terms of their brain wave oscillations between each electrode pair, while the AEC measure indicates their correlation in terms of their amplitude.

To reflect effective communication between brain regions, a mean connectivity profile analysis was performed. The Kruskal-Wallis test showed significant differences in mean connectivity, particularly within the Alpha band for all connectivity measures and ISPC measures across all bands (Fig. 2). Notably, in the Alpha-ISPC study, these significant differences were concentrated in connections inside the frontal lobe and between the frontal and other brain regions. Multiple comparisons further highlighted the distinct connectivity profiles of AD and FD. Both dementia subtypes mutually exhibited strong whole-brain hypoconnectivity in alpha-band wPLI and AEC measures, with subtle differences between the two subtypes. Similarly, a decrease in mean connectivity was observed across all dementia subtypes compared to HC in both Alpha and Beta-band ISPC studies, primarily localized to frontal-frontal and frontal-occipital connections. AD demonstrated a whole-brain hyperconnectivity in Delta-ISPC studies compared to HC and FD. In the Theta-ISPC study, AD also showed general hyperconnectivity but was relatively preserved in Frontal-Frontal and Frontal-Occipital connections. In contrast, whole-brain hypoconnectivity was found specifically for the FD group in most of the connections in the Theta-ISPC study.

The variance of brain connectivity revealed distinct and significant patterns, particularly in the Alpha-wPLI and Alpha-AEC studies (Fig. 3). The post-hoc analyses then showed a significantly lower variance of connectivity in alpha-band wPLI and AEC studies for both AD and FD groups compared to HC. However, no significant difference was found between the two dementia subtypes. The lower variance was observed in the Alpha-ISPC study, although less pronounced in frontal-frontal and frontal-occipital connections. Distinctively, AD has a lower variance of connectivity in some connections across the brain compared to FD and HC in the wPLI and AEC measures of the Delta band.

The skewness analysis revealed differences mainly in frontal-frontal and frontal-occipital connections within the Alpha-ISPC study (Fig. 4). Pairwise comparisons demonstrated that both AD and FD exhibited positively skewed connectivity across all measures in the Alpha band and Beta-ISPC studies; however, no significant differences in skewness were observed between AD and FD groups.

Shannon entropy was applied to assess the complexity of brain connectivity patterns. Our analysis demonstrated significant differences in ISPC measure studies and Alpha band studies (Fig. 5). Subsequent post-hoc analyses revealed that the Shannon entropy of connectivity was lower in the Alpha band for all measures, as

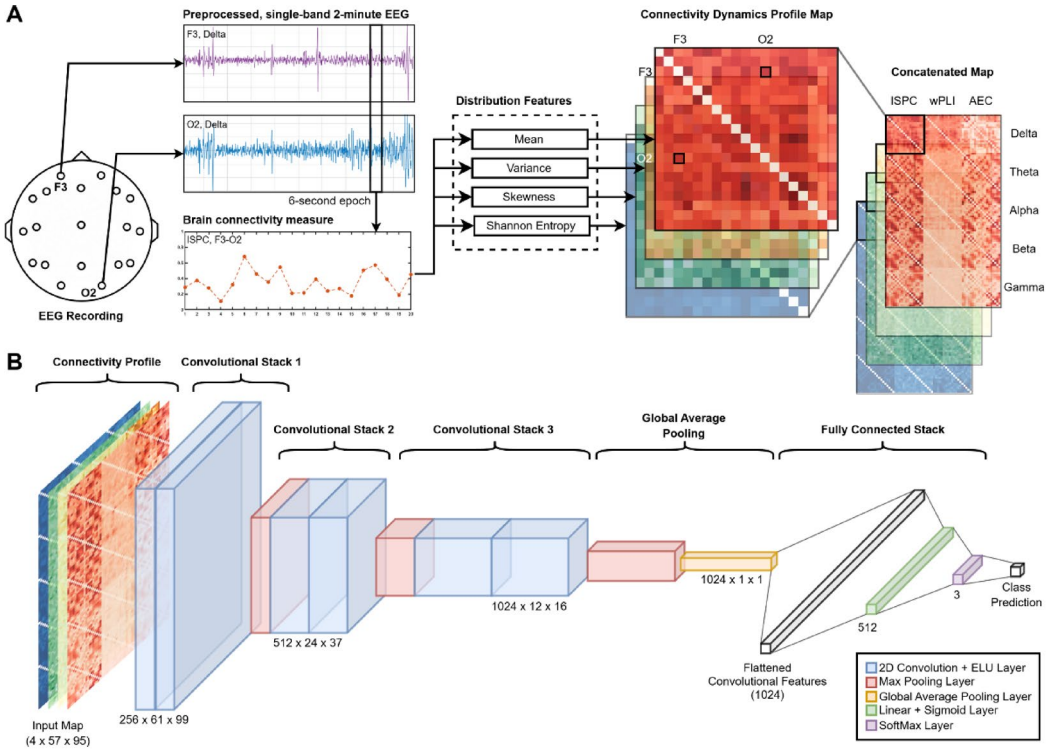

Fig. 1. The workflow of EEG connectome profile-based convolutional neural network approach for dementia subtype classification. (**A**) Derivation of connectivity dynamics profile map from EEG recording. (**B**) The convolutional neural network-based architecture of our classification model.

well as for the ISPC measure in the Beta and Gamma bands of both the AD and FD groups. However, AD has a particularly lower entropy, compared to FD, in the Alpha-ISPC study. In distinguishing dementia subtypes, AD exhibited significantly higher complexity of connectivity in the Delta-ISPC study, while the FD group displayed lower entropy of connectivity in the Theta-ISPC study.

In addition to mean, variance, skewness, and Shannon entropy, we also included standard deviation (SD), kurtosis, and higher-order central and standardized moments in our analysis. While these additional features generally corroborated the trends observed in the primary features (e.g., SD mirrored variance, and third-order central moments aligned with skewness), no significant differences were found in kurtosis or higher-order moments.

Dementia subtypes classification performance

A CNN model was developed to distinguish dementia subtypes using EEG data. Our model used dynamic features obtained from the previous analysis of brain connectivity measures. As stated in the Methods section, the statistical features were converted into images of brain connectivity maps to provide information as input for the models regarding brain connectivity across three connectivity measures and five brain frequency bands.

For the multiclass classification task, models were trained to classify trials into three groups: AD, FD, or HC. Using dynamic features of whole-trial brain connectivity maps, the model performed at a mean accuracy of 93.5% ± 3.4% (Table 1).

To gain an understanding of the impact of frequency bands and connectivity measures, we conducted additional analyses using partial input. In the band-wise analysis, the models were trained on data from specific frequency bands. Among the band-wise models, low-frequency bands such as the Delta and Theta bands achieved superior accuracy of 91.1% ± 6.0% and 92.3% ± 3.9%, respectively, compared to the high-frequency Gamma band, which performed at the lowest accuracy of 85.5% ± 6.5%. In the measure-wise analysis, where individual connectivity measures were applied, the models with ISPC or AEC achieved comparable accuracy of 90.5% ± 5.2% and 89.8% ± 5.2%, respectively. In contrast, the wPLI model was relatively inaccurate and unstable, with an accuracy of 83.7% ± 11.4%. For the single band and measure study, where models rely solely on specific frequency bands or connectivity measures, the results showed limited performance, with mean accuracies ranging from 38.2 to 67.6%.

To prove that the dynamic feature approach can improve classification performance, we conducted a comparative classification task on the same model architecture but employed only the static feature (mean) of brain connectivity. The results showed that it can perform with a mean accuracy of up to 91.6% using the wPLI measure. For the whole trial model, the accuracy dropped to 87.0% ± 3.9%. However, while the models using band-wise and measure-wise inputs showed a decrease in accuracy, the single band and measure models

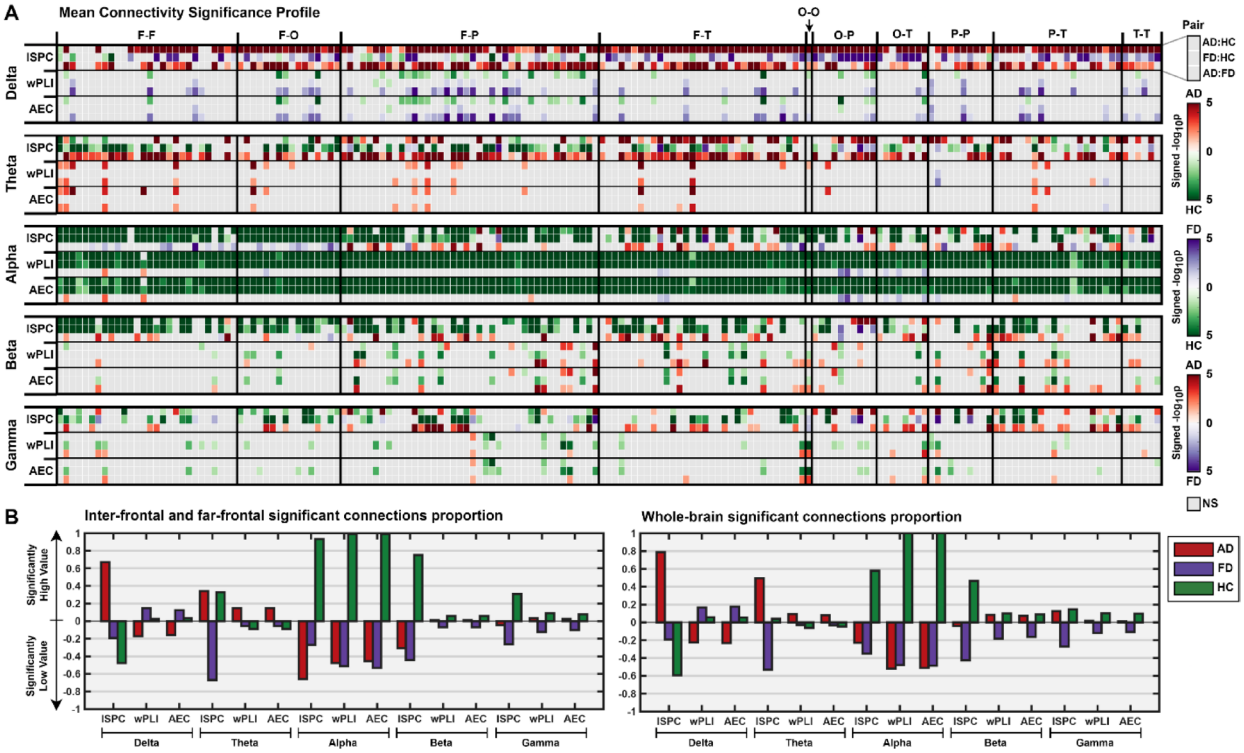

Fig. 2. Mean connectivity between dementia subtypes and healthy control. (**A**) Mean connectivity significance profile. Each color represents the preference classification group from the significance of mean connectivity in a brain wave band and feature between an electrode pair. The color intensity corresponds to the p-value of difference from the post-hoc analysis in a negative logarithmic scale. (**B**) Proportion of significant connections. Each bar represents the proportion of electrode pairs with a higher value of mean connectivity in the brain wave band and the feature preferring a specific group minus the proportion of electrode pairs that suggest otherwise. The proportion of + 1 indicates that the mean connectivity for the group in the study is higher than other comparative groups in all connections, while the proportion of − 1 indicates that the value is lower than other comparative groups in all connections. The inter-frontal and far-frontal refer to frontal-frontal and frontal-occipital connections, respectively. AD = Alzheimer's Disease; FD = Frontotemporal Dementia; HC = Healthy Control; NS = Not significant; F = Frontal electrodes; O = Occipital electrodes; P = Parietal electrodes; T = Temporal electrodes.

performed better in various cases with larger input models, especially models using ISPC and AEC measure-related data.

The pairwise classification was used to differentiate dementia from healthy controls as well as between the subtypes themselves, as shown in Table 1. For the AD/HC classification, the best model achieved an accuracy of 97.8% ± 1.8% using data from the ISPC measure. The model using the AEC measure demonstrated a comparable accuracy of 95.4% ± 1.6%, in contrast to the model using the wPLI measure, which performed at only 91.8% accuracy with a high standard deviation of 9.5%. For band-wise models, they exhibited comparable performance, ranging from 93.1 to 97.4% accuracy for the Delta and Beta bands, respectively. The whole trial model achieved an accuracy of 93.7% ± 6.2%. Notably, for single input models, the model using Alpha-ISPC and Alpha-AEC data reached high accuracies of 91.6% and 90.5%, respectively.

For the classification between FD and HC, the best-performing model used AEC measure data to achieve an accuracy of 96.7% ± 3.3%. Using ISPC and wPLI measures, the model showed comparable mean accuracies of 96.4% and 95.1%, respectively. For the band-wise study, the model utilizing Theta band data showed a high accuracy of 96.4% ± 3.3%. The model using whole trial data achieved a lower accuracy of 93.4% ± 6.2%.

In the classification between dementia subtypes (AD and FD), our best-performing model achieved an accuracy of 97.4% ± 3.4% using AEC measure data. The wPLI measure model also showed equivalent performance at 96.7% ± 5.6% accuracy. For the band-wise study, the model using the Theta and Gamma bands showed relatively high accuracy, compared to other bands, at 96.1% and 97.1%, respectively. Using whole trial data, the model could only perform at 93.8% accuracy.

To understand how our proposed model extracted meaningful features in the classification, we displayed the model's convolutional features using the t-SNE visualization method. The extracted features of our best-performing models are displayed in well-separating clusters in every classification task (Fig. 6 and Supplementary Figures S1-S3), indicating that models learned well distinctive patterns of brain connectivity dynamics. Additionally, convolutional features extracted from trials of the same subject appeared closer together or

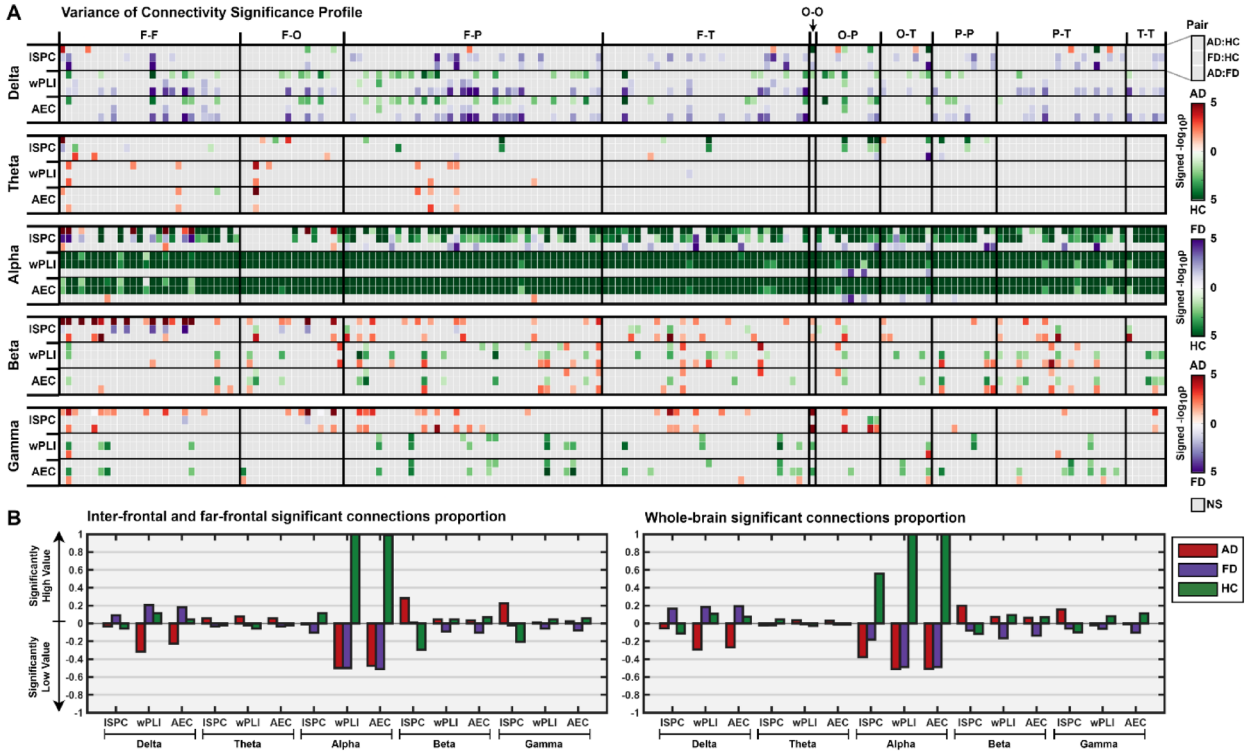

Fig. 3. Variance of connectivity between dementia subtypes and healthy control. (**A**) Variance of connectivity significance profile. Each color represents the preference classification group from the significance of variance of connectivity in a brain wave band and feature between an electrode pair. The color intensity corresponds to the p-value of difference from the post-hoc analysis in a negative logarithmic scale. (**B**) Proportion of significant connections. Each bar represents the proportion of electrode pairs with a higher value of the variance of connectivity in the brain wave band and the feature preferring a specific group minus the proportion of electrode pairs that suggest otherwise. The proportion of + 1 indicates that the variance of connectivity for the group in the study is higher than other comparative groups in all connections, while the proportion of − 1 indicates that the value is lower than other comparative groups in all connections. The inter-frontal and far-frontal refer to frontal-frontal and frontal-occipital connections, respectively. AD = Alzheimer's Disease; FD = Frontotemporal Dementia; HC = Healthy Control; NS = Not significant; F = Frontal electrodes; O = Occipital electrodes; P = Parietal electrodes; T = Temporal electrodes.

superimposed in the visualization, indicating that the model consistently identified and represented the unique connectivity profiles of individual subjects.

To assess the impact of excluding outliers, we performed the model training for the multiclass classification task (AD, FD, and HC) on the entire dataset without outlier rejection. The results, using whole trial data, showed a significant decrease in accuracy and stability, dropping to 59.7% ± 10.3%. Surprisingly, the model trained on the outlier-rejected data can maintain an accuracy of 89.6% ± 0.5% when classifying the whole dataset that included the outliers. By examining the prediction behavior of outlier trials, inferred from the model trained without outlier data, t-SNE visualization of the multiclass classification model demonstrated that certain outlier subjects are consistently misclassified: some outlier trials labeled as HC are plotted as the AD group, while most of the outliers in the FD group also appear as AD. Remarkably, a similar pattern was observed in the binary classification task as well.

Discussion

This research focused on exploring the dynamic features of brain connectivity profiles among dementia subtypes based on resting-state EEG recordings as electrical biomarkers to enhance dementia diagnosis using deep learning frameworks. By conducting statistical analysis, we identified distinct connectivity patterns associated with dementia. Our models, enhanced with the proposed dynamic features, achieved high accuracy and outperformed the models utilizing static features in dementia classification tasks.

Our findings suggest a common characteristic of dementia: a consistent reduction in whole-brain phase and amplitude connectivity within the Alpha band, with infrequent instances of normal or hyperconnectivity. The positive skewness observed in phase-based connectivity patterns indicates a concentration of lower connectivity values, implying disrupted or impaired communication within the frontal lobe and far-frontal connections. These findings align with previous functional magnetic resonance imaging (fMRI) studies of the default mode network (DMN)[18,19] and neuropathological findings specific to AD[20]. In addition, a study combining EEG and fMRI demonstrated a reduction in frontal-caudal connectivity in AD patients[21], supporting our findings in

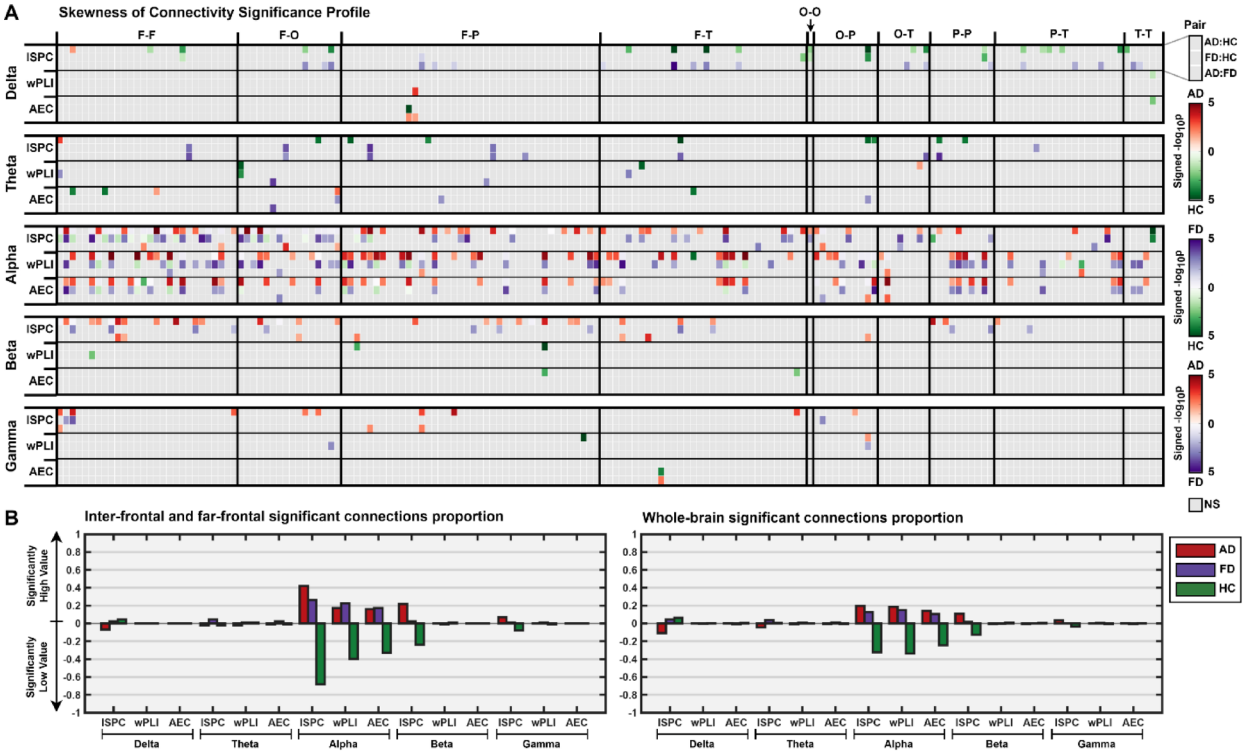

Fig. 4. Skewness of connectivity between dementia subtypes and healthy control. (**A**) The skewness of connectivity significance profile. Each color represents the preference classification group from the significance of skewness of connectivity in a brain wave band and feature between an electrode pair. The color intensity corresponds to the p-value of difference from the post-hoc analysis in a negative logarithmic scale. (**B**) Proportion of significant connections. Each bar represents the proportion of electrode pairs with a higher value of skewness of connectivity in the brain wave band and the feature preferring a specific group minus the proportion of electrode pairs that suggest otherwise. The proportion of + 1 indicates that the skewness of connectivity for the group in the study is higher than other comparative groups in all connections, while the proportion of − 1 indicates that the value is lower than other comparative groups in all connections. The inter-frontal and far-frontal refer to frontal-frontal and frontal-occipital connections, respectively. AD = Alzheimer's Disease; FD = Frontotemporal Dementia; HC = Healthy Control; NS = Not significant; F = Frontal electrodes; O = Occipital electrodes; P = Parietal electrodes; T = Temporal electrodes.

frontal-occipital connections. A strong relationship between EEG and fMRI, involving the DMN, has been reported[22], further validating our approach of utilizing distribution features to probe the importance of brain connectivity dynamics.

Distinct phase-based connectivity profiles can differentiate dementia subtypes. AD patients exhibited significantly higher mean and Shannon entropy values in Delta-band connections compared to HC; on the contrary, FD patients showed significantly lower mean value and complexity of phase-based connectivity in the Theta, Beta, and Gamma bands. Although our findings may appear counterintuitive to the EEG studies reporting a decrease in lagged phase synchronization in AD patients[23], recent research has revealed increased Delta-related cross-coupling connectivity in AD compared to FD[24]. Additionally, fMRI studies have suggested an increase in functional connectivity of specific AD networks[25], aligning with the report of the strong relationship between EEG and fMRI connectivity dynamics in the Delta band[22]. Our study showed that the dynamic changes in AD were unique to FD. However, further investigation is needed to fully understand these connectivity dynamics, particularly within the Delta and Theta bands.

Even though wPLI is a phase-based connectivity measure, its profile patterns in most statistical analyses resemble those of AEC, an amplitude-based connectivity measure. This similarity can be attributed to the derivation of wPLI from cross-spectral density, which involves the product of amplitude and phase differences. Consequently, amplitude influences the weighting of wPLI, contributing to the observed similarities between wPLI and AEC.

For the classification tasks, our CNN framework achieves impressive accuracy in both multiclass and pairwise classifications. By integrating dynamic features of brain connectivity, the accuracy of the classification models improved compared to the model that utilized only static features.

The whole-trial classifier generally outperformed band-wise and measure-wise models when classifying multiple groups. However, the best-performing models in pairwise classifications come from measure-wise models, which greatly surpassed whole-trial models in both accuracy and stability. We hypothesize that this optimal performance results from a balanced input for training deep learning models. While incorporating all

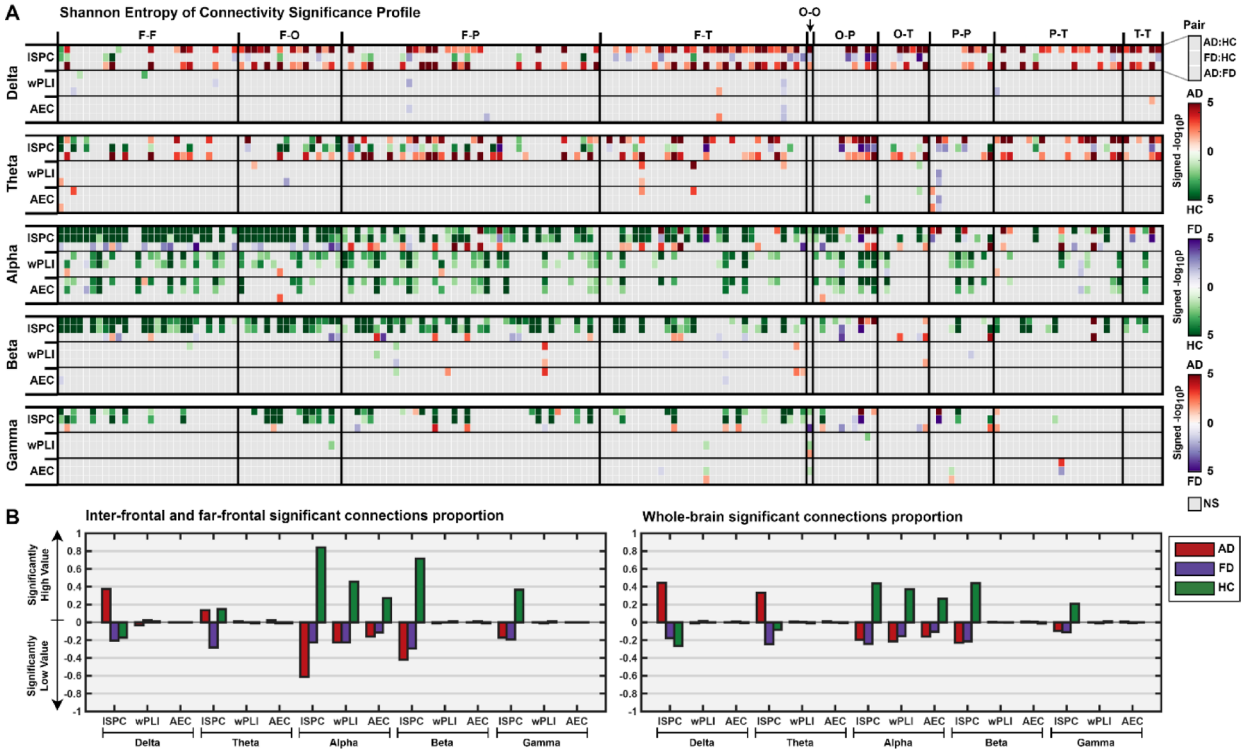

Fig. 5. Shannon entropy of connectivity between dementia subtypes and healthy control. (**A**) Shannon entropy of connectivity significance profile. Each color represents the preference classification group from the significance of Shannon entropy of connectivity in a brain wave band and feature between an electrode pair. The color intensity corresponds to the p-value of difference from the post-hoc analysis in a negative logarithmic scale. (**B**) Proportion of significant connections. Each bar represents the proportion of electrode pairs with a higher value of Shannon entropy of connectivity in the brain wave band and the feature preferring a specific group minus the proportion of electrode pairs that suggest otherwise. The proportion of + 1 indicates that the Shannon entropy of connectivity for the group in the study is higher than other comparative groups in all connections, while the proportion of − 1 indicates that the value is lower than other comparative groups in all connections. The inter-frontal and far-frontal refer to frontal-frontal and frontal-occipital connections, respectively. AD = Alzheimer's Disease; FD = Frontotemporal Dementia; HC = Healthy Control; NS = Not significant; F = Frontal electrodes; O = Occipital electrodes; P = Parietal electrodes; T = Temporal electrodes.

data as input provides a broader context, it can also lead to overcomplexity and poor generalization[26], whereas insufficient input may hinder the model's ability to classify confidently.

Comparing the model inputs of deep learning, single-input model performances align with statistical analysis. However, while the profiles of wPLI and AEC measure-related models are similar, their performances appear to differ significantly. We hypothesize that AEC-measure connectivity matrices exhibit dependency patterns between electrode pairs, which may convey information to the classification model that is undetectable through individual connection analysis, thereby enhancing classification performance. We observed that the classification performance can be improved by integrating wPLI measure-related inputs into a measure-wise wPLI model. This supports the hypothesis that interactions can be identified across bands as well. These findings highlight the necessity for further investigation to examine the connectivity dynamics as a network. Future studies should consider employing novel techniques, such as graph convolutional networks[27], topological models such as N-body orbital graphs[28] or graphical features[29] to explore the complex interactions between brain regions.

Several comparative studies were conducted on the same dataset (Table 2). Overall, the performance of our models outperformed most comparative models using the cross-validation scheme[30–36] in both multiclass classification tasks and binary classification. Only studies with test-train split validation[37,38] and the study using topological features with an ensemble learning model[28] that reported higher performance. While most deep learning-based studies, including this work, proposed custom CNN architecture for their classification task, comparative studies of pre-trained CNN models are needed. As pre-trained models have improved brain-computer interface classification[39], future work should assess their potential for dementia diagnosis.

The primary limitation of this study is that the dataset is restricted to a single-centered source with a limited number of trials, which may result in overfitting and diminished generalization[9]. As highlighted in the earlier literature, studies with small sample sizes tend to lack versatility and struggle to generalize across subjects with differing amounts of training data[40]. The imbalance in the dataset, where the FD group had a significantly shorter recording duration compared to the AD and HC groups, is another limitation that directly impacted

	AD/FD/HC				AD/HC		FD/HC		AD/FD	
	Dynamic features		Static feature							
Model inputs	Accuracy	F1 score	Accuracy	F1 score	Accuracy	F1 score	Accuracy	F1 score	Accuracy	F1 score
Whole trial	**93.5 (3.3)**	**93.4 (3.5)**	87.0 (3.9)	86.9 (3.8)	93.7 (6.2)	93.6 (6.4)	93.4 (6.2)	93.3 (6.4)	93.8 (9.2)	93.8 (9.3)
Delta band	91.1 (6.0)	90.9 (6.2)	85.9 (5.0)	85.7 (5.0)	93.1 (6.1)	93.0 (6.3)	91.7 (9.4)	91.4 (9.9)	92.6 (7.2)	92.5 (7.3)
Theta band	92.3 (3.9)	92.3 (3.8)	88.5 (5.5)	88.5 (5.3)	95.0 (5.1)	95.0 (5.2)	92.3 (3.6)	92.2 (3.7)	96.1 (4.5)	96.1 (4.5)
Alpha band	89.9 (3.8)	89.7 (3.8)	86.5 (9.2)	86.1 (9.6)	95.4 (4.6)	95.4 (4.6)	89.5 (9.1)	89.2 (9.5)	94.3 (7.2)	94.2 (7.4)
Beta band	88.2 (6.4)	88.2 (6.4)	86.5 (4.3)	86.4 (4.2)	97.4 (3.6)	97.4 (3.6)	96.4 (3.3)	96.4 (3.3)	93.1 (7.0)	92.9 (7.3)
Gamma band	85.8 (6.5)	85.7 (6.6)	84.8 (8.2)	84.4 (8.6)	96.3 (3.3)	96.3 (3.4)	93.0 (8.3)	92.7 (8.8)	97.1 (2.7)	97.1 (2.7)
ISPC measure	90.5 (5.2)	90.4 (5.2)	87.0 (4.8)	86.6 (5.2)	**97.8 (1.8)**	**97.8 (1.8)**	96.4 (4.8)	96.3 (4.9)	92.3 (6.4)	92.2 (6.6)
wPLI measure	83.7 (11.4)	83.4 (11.6)	**91.6 (3.8)**	**91.6 (3.8)**	91.8 (9.5)	91.8 (9.5)	95.1 (4.2)	95.1 (4.2)	96.7 (5.6)	96.6 (5.6)
AEC measure	89.8 (5.2)	89.7 (5.1)	88.5 (5.9)	88.5 (5.8)	95.4 (1.6)	95.4 (1.6)	**96.7 (3.3)**	**96.7 (3.4)**	**97.4 (3.4)**	**97.4 (3.4)**
Delta-ISPC	64.5 (5.7)	64.1 (6.1)	85.4 (6.8)	85.2 (6.8)	81.0 (2.9)	80.7 (3.2)	75.5 (6.2)	75.2 (6.4)	69.7 (3.6)	69.2 (4.0)
Delta-wPLI	42.9 (7.3)	33.7 (12.8)	47.2 (5.3)	43.1 (7.2)	58.4 (7.5)	56.2 (9.7)	63.1 (5.2)	59.7 (7.1)	58.6 (9.8)	53.6 (12.9)
Delta-AEC	64.7 (11.9)	64.6 (12.2)	79.8 (9.8)	79.5 (10.0)	83.0 (3.8)	82.9 (3.8)	72.8 (8.0)	72.4 (8.3)	77.0 (5.2)	76.5 (5.7)
Theta-ISPC	60.5 (7.5)	60.5 (7.5)	86.0 (6.4)	86.0 (6.4)	86.8 (3.2)	86.7 (3.2)	72.5 (8.3)	72.4 (8.4)	72.2 (6.3)	71.4 (7.1)
Theta-wPLI	49.2 (7.7)	47.7 (8.1)	57.7 (7.9)	57.3 (7.8)	69.1 (9.1)	69.0 (9.3)	59.8 (6.0)	56.0 (10.4)	65.6 (6.7)	64.9 (6.8)
Theta-AEC	62.2 (8.2)	61.7 (8.2)	85.1 (8.5)	85.1 (8.4)	87.8 (1.9)	87.7 (1.9)	77.1 (6.8)	77.0 (6.8)	75.8 (6.4)	75.6 (6.4)
Alpha-ISPC	67.6 (13.0)	66.6 (13.4)	85.1 (7.2)	84.9 (7.4)	91.6 (4.9)	91.6 (5.0)	83.5 (7.4)	83.2 (7.7)	69.2 (8.3)	67.7 (9.8)
Alpha-wPLI	59.0 (7.5)	58.5 (8.1)	63.6 (11.1)	62.8 (10.8)	81.9 (4.1)	81.7 (4.2)	76.6 (9.1)	75.8 (9.9)	63.4 (4.6)	62.8 (4.3)
Alpha-AEC	65.5 (6.6)	64.0 (6.5)	85.9 (6.3)	86.0 (6.2)	90.5 (5.7)	90.5 (5.8)	85.4 (6.6)	85.4 (6.7)	74.4 (9.5)	74.2 (9.5)
Beta-ISPC	66.5 (7.4)	65.9 (8.2)	77.6 (13.3)	77.6 (13.4)	88.2 (3.3)	88.1 (3.4)	77.1 (3.3)	76.6 (3.8)	65.9 (8.3)	65.2 (8.6)
Beta-wPLI	38.2 (3.4)	28.1 (6.6)	51.9 (7.8)	51.3 (8.2)	52.9 (3.7)	50.1 (5.6)	61.3 (4.4)	58.4 (6.5)	54.8 (4.7)	50.8 (6.3)
Beta-AEC	61.2 (4.1)	61.1 (4.1)	84.6 (7.2)	84.4 (7.6)	84.4 (4.1)	84.4 (4.1)	80.3 (6.0)	80.3 (6.0)	69.7 (6.1)	69.1 (6.1)
Gamma-ISPC	58.8 (6.5)	58.2 (7.1)	78.5 (4.1)	78.3 (4.1)	71.9 (5.0)	71.0 (5.4)	71.1 (4.6)	70.9 (4.5)	62.4 (4.8)	61.6 (5.6)
Gamma-wPLI	40.7 (8.1)	34.7 (11.9)	52.3 (10.4)	48.7 (16.6)	53.5 (4.2)	49.1 (8.2)	60.1 (7.8)	58.7 (8.9)	56.7 (7.2)	52.1 (12.2)
Gamma-AEC	56.7 (4.7)	56.2 (4.7)	75.7 (7.0)	75.5 (7.1)	72.9 (7.3)	72.6 (7.4)	74.4 (6.8)	74.0 (7.2)	73.5 (8.2)	72.6 (9.7)

Table 1. Performance metrics of models in multiclass classification using combinations of brain wave bands and connectivity measures. Each cell displays the mean percentage and standard deviation (SD) of the accuracy and F1 score across five-fold cross-validation. The best mean accuracy and F1 score for each classification task were highlighted in bold. AD, Alzheimer's disease; FD , frontotemporal dementia; HC , healthy control.

the classification performance involving FD. Although the oversampling technique was implemented to address this issue, its effects were limited[41]. Thus, acquiring additional EEG data, particularly from FD and other rare dementia subtypes, is essential for a deeper understanding of their unique characteristics and enhancing model performance. This underscores the significance of assessing model performance across a variety of subjects and datasets to ensure dependable translation to clinical environments. Therefore, future studies utilizing larger datasets from multiple clinical centers are advised. Furthermore, to adapt our approach to clinical settings, we recommend employing transfer learning techniques to fine-tune our model with local datasets, ensuring enhanced performance and better adaptability.

Although our study focused on resting-state EEG recordings, dementia primarily impacts higher cortical functions and involves impairments in neurological tasks. Therefore, incorporating task-based EEG data could provide deeper insights into the dynamic changes in brain connectivity associated with diseases[42]. We hypothesize that examining brain connectivity dynamics during cognitive tests could provide more valuable information for diagnosis, evaluating disease severity, and potentially identifying personalized neurological deficits.

Conclusion

This study demonstrated the feasibility of using dynamic EEG connectivity features to characterize brain connectivity changes in dementia and distinguish between its subtypes. We described mutual alterations in dementia as a generalized and consistent disruption of connectivity in the Alpha band. Distinct characteristics were identified through generalized phase hyperconnectivity with increased complexity in the Delta band for AD, along with disrupted phase-based connectivity in the Theta, Beta, and Gamma bands for FD. Our proposed deep learning model, enhanced with dynamic features, outperformed static feature models and most comparative studies. This work advances dementia research by establishing a high-performance deep-learning framework that leverages dynamic EEG connectivity as potential biomarkers. Expanding the dataset and incorporating multi-center data could improve model generalizability, while task-based EEG studies may enhance diagnostic insights. Ultimately, this approach could facilitate automated, non-invasive, and cost-effective early dementia detection, improving patient management and treatment outcomes.

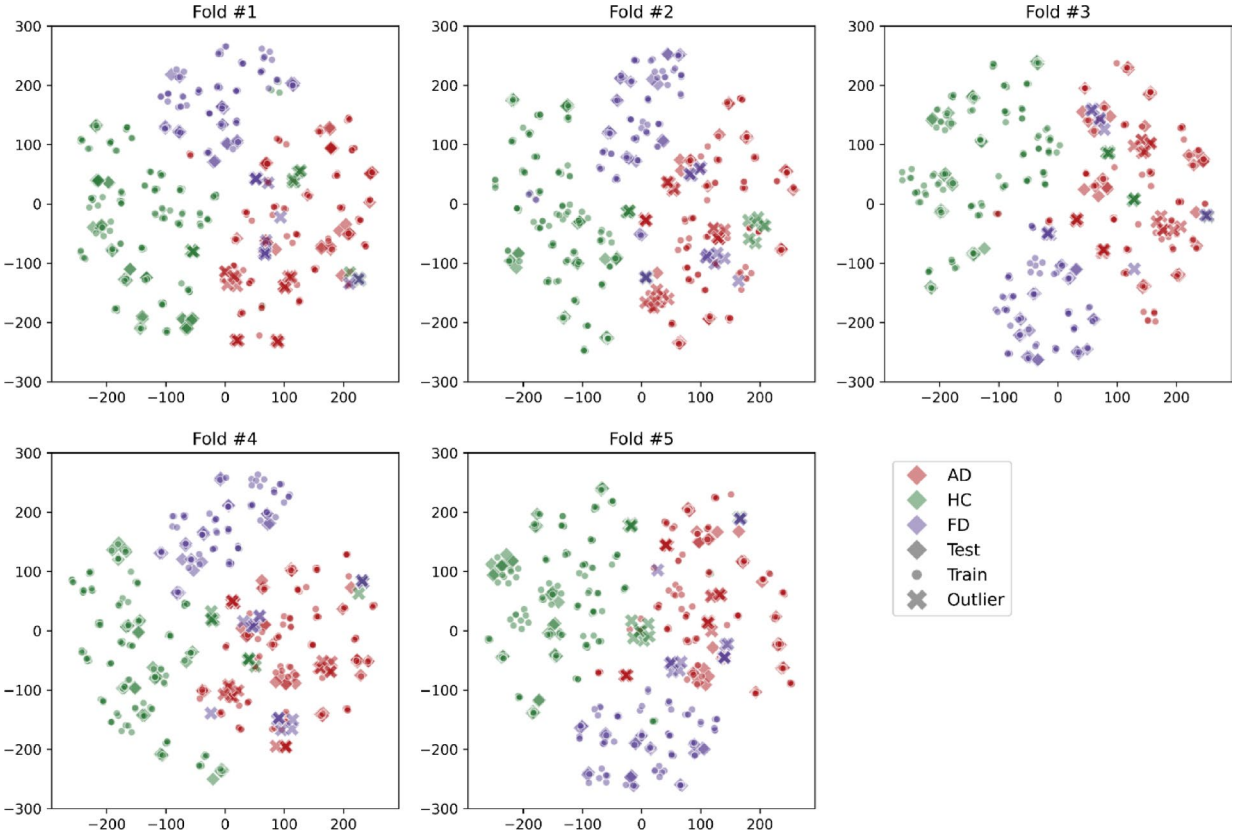

Fig. 6. Two-dimensional t-SNE visualization of convolutional features of the instance-wise model for AD/FD/HC task. A uniform jitter of diameter 5 was added to provide a better view of overlapping data points. The color of the data point represents an actual labeled group of each trial. Data points in the test set and training set, corresponding to each fold, are displayed in diamonds and points, respectively. Outliers are also displayed in cross symbols. AD = Alzheimer's Disease; FD = Frontotemporal Dementia; HC = Healthy Control.

Methods

EEG recordings

EEG data were obtained from the publicly available OpenNeuro Dataset ds004504[3]. This dataset included resting-state, eyes-closed EEG recordings from 88 participants: 36 patients with AD, 23 patients with FD, and 29 HC subjects. Participants' ages ranged from 44 to 79 years, with an average age of 66 years. The participant characteristics for each group are displayed in Supplementary Table S1. EEG data were collected using a Nihon Kohden 2100 system in a standard 10–20 configuration at a sampling rate of 500 Hz. The total durations for the AD, FD, and HC groups were 485.5, 276.5, and 402 minutes, respectively.

Data pre-processing

The EEG data were processed and analyzed using custom-written code in MATLAB 2024a (MathWorks, MA). Common average referencing was applied to establish a common ground for signal comparison[43]. A 0.5-Hz high-pass Butterworth filter was used to remove low-frequency noise and baseline drift. The Artifact Subspace Reconstruction (ASR)[44] was employed to identify and remove 0.5-second epochs with power levels exceeding 20 times SD. The Independent Component Analysis (ICA)[45] was then carried out to extract 19 independent components from the 19 EEG channels. ICLabel[46] and the wavelet-enhanced ICA (wICA) algorithm[47] were utilized to eliminate identified artifacts (e.g., eye movements, jaw movements). The preprocessed EEG signals were divided into frequency bands (Delta: 0.5–4 Hz, Theta: 4–8 Hz, Alpha: 8–13 Hz, Beta: 13–25 Hz, and Gamma: 25–45 Hz) using Butterworth bandpass filters for subsequent analysis.

Brain connectivity measures

The connectivity measures were calculated from six-second, non-overlapping epochs of Hilbert-transformed EEG recordings, considering all 171 electrode pairs within specific frequency bands. This analysis investigates the functional interactions between brain regions across frequency bands.

Inter-site phase clustering

The ISPC is the phase-based connectivity measure that quantifies the degree of phase synchronization between two EEG signals[48]. It is computed by averaging the phase difference between the two electrodes, p and q, over a specific time window. To calculate the ISPC for a given epoch, we first obtained the phase angles, $\varphi_p(t)$

References	Feature(s)	Algorithm(s)	Validation	Classification Task	Accuracy
Our Method	Functional Connectivity	CNN	5-fold CV	AD/FD/HC	93.5%
				AD/HC	97.8%
				FD/HC	96.7%
				AD/FD	97.4%
Miltiadous et al.[31]	Relative Band Power, Spectral Coherence Connectivity	DICE-net	Leave-one-subject-out	AD/HC	83.28%
				FD/HC	74.96%
Chen et al.[30]	Time domain, Frequency domain	ViT-CNN	10-fold CV	AD/FD/HC	76.01%
Zheng et al.[32]	Spectral features, Complexity, Synchronization	RF	Leave-one-subject-out	AD/HC	95.86%
Puri et al.[33]	RMS, Hjorth coefficients, Power Spectrum, Complexity	SVM	10-fold CV	AD/HC	98.90%
			Leave-one-subject-out		96.56%
Zheng et al.[34]	Multi-Threshold Recurrence Rate Plots	SVM	Leave-one-out	AD + FD/HC	86.36%
				AD/HC	87.69%
				FD/HC	82.69%
				AD/FD	72.88%
Yang et al.[37]	Microstate features	SVM	70% Train / 30% Test Split	AD/HC	99.22%
		kNN			96.35%
		RF			99.88%
		LR			99.01%
Puri et al.[38]	Time domain	LEADNet	70% Train / 10% Validate / 20% Test Split	AD/HC	99.24%
Rostamikia et al.[35]	Time domain features, Frequency domain features, Connectivity, Complexity	SVM	10-fold CV	AD + FD/HC	93.5%
				AD/FD	87.8%
Ma et al.[36]	Mutual Information	SVM	Leave-one-out	AD/HC	76.9%
				FD/HC	90.4%
				AD/FD	96.6%
Barua et al.[28]	N-Body orbital graph	Ensemble kNN	10-fold CV	AD/FD/HC	99.64%

Table 2. Comparative studies and performance machine learning-based detection of dementia subtypes using the same dataset. CV, cross-validation; ViT, visual transformer; RF, random forest; SVM, support vector machine; kNN, k-nearest neighbor; LR, logistic regression; RMS, root mean square; AD, Alzheimer's disease; FD, frontotemporal dementia; HC, healthy control.

and $\varphi_q(t)$, for each electrode at each time point t within the epoch. The ISPC was then computed using the following equation:

$$ISPC(T,p,q) := \left| \frac{1}{n(T)} \cdot \sum_{t \in T} e^{i\left(\phi_p(t) - \phi_q(t)\right)} \right| \tag{1}$$

where T represents the set of time points within the epoch, ISPC value ranges from 0 to 1, with 1 indicating perfect phase synchronization, meaning that the signals are consistently in phase.

Weighted phase-lag index

The wPLI is a modified version of the phase lag index that quantifies the directionality of functional interactions between brain regions. It measures the extent to which the phase of one signal consistently leads or lags the phase of another[49]. The wPLI was derived from the cross-spectral density, defined as $S_{pq}(t) := \psi_p(t) \cdot \psi_q^*(t)$ where $\psi_p(t)$ is the complex wave of electrode p and $\psi_q^*(t)$ is the complex conjugate wave of electrode q at time point t. The wPLI was then obtained from the equation below:

$$wPLI(T,\ p,q) := \frac{\frac{1}{n(T)} \cdot \sum_{t \in T} \left|\mathrm{Im}\left(S_{pq}(t)\right)\right| \mathrm{sgn}\left(\mathrm{Im}\left(S_{pq}(t)\right)\right)}{\frac{1}{n(T)} \cdot \sum_{t \in T} \left|\mathrm{Im}\left(S_{pq}(t)\right)\right|} \tag{2}$$

where T represents the set of time points within the epoch. $\mathrm{Im}(z)$ indicates the imaginary part of the complex number z and $\mathrm{sgn}(x)$ is the signum function, which returns – 1, 0, or 1 based on the sign of x. The wPLI value ranges from 0 to 1, with higher values indicating stronger directed functional connectivity between the two electrodes.

Amplitude envelope correlation

The AEC is an amplitude-based connectivity measure that quantifies the synchronization of amplitude fluctuations between two EEG signals[50]. To calculate the AEC, Pearson's correlation (ρ) was calculated on amplitude envelopes as follows:

$$AEC\,(T,\ p,q) := \frac{\sum_{t\in T}\left(|\psi_p(t)|-\mu_p\right)\left(|\psi_q(t)|-\mu_q\right)}{\sqrt{\sum_{t\in T}\left(|\psi_p(t)|-\mu_p\right)^2\cdot\sum_{t\in T}\left(|\psi_q(t)|-\mu_q\right)^2}} \tag{3}$$

where T is the set of time points within the epoch. $\psi_p(t)$ and $\psi_q(t)$ are the complex waves of electrode p, and q, respectively. μ_p and μ_q refer to the mean of amplitude envelope of complex waves of electrode p, and q, respectively. The AEC value ranges from −1 to 1. A value of 1 indicates strong amplitude synchronization, meaning that the amplitudes of the two signals fluctuate in unison. Conversely, the value of -1 indicates strong anti-synchronization, meaning that the amplitudes of the two signals fluctuate in opposite directions.

Statistical features extraction

To extract meaningful statistical features, we segmented the EEG recordings of each subject into two-minute overlapping samples (containing 20 epochs) with a maximum overlap of 50%. Statistical features, including the mean, variance, skewness, and Shannon entropy, were calculated from the ISPC, wPLI, and AEC. These features provide insights into brain connectivity patterns' distribution, variability, and randomness. These features were then employed to determine the unique connectivity profiles associated with each dementia subtype.

Analysis of connectivity profiles

To analyze the connectivity profiles specific to dementia subtypes, the statistical measures of brain connectivity among AZ, FD, and HC were compared using the Kruskal-Wallis's test to assess group differences for each electrode pair, frequency band, and connectivity measure. The significance level was set at 0.05. The effect size was reported as Eta-squared to quantify the magnitude of the differences. To investigate whether specific features were associated with dementia subtypes, we performed Dunn-Sidak corrected post-hoc analyses, which included pairwise comparisons of AD/HC, FD/HC, and AD/FD. The effect size for the post-hoc tests was indirectly reported as signed p-values, providing insights into both the significance of the differences and the direction of the effects.

Dementia subtype classification

Connectivity profile maps

The extracted statistical features were used to create connectivity profile maps. The map was a 19×19 matrix representing the statistical features of a specific connectivity measure and brain wave band between all electrode pairs (Fig. 1). By incorporating four channels for each statistical feature, we expanded the feature maps to a size of $4\times19\times19$.

The connectivity profile maps were concatenated laterally in three different schemes: band-wise, feature-wise, and whole trial. In the band-wise scheme, the feature maps for all three statistical features within a specific frequency band were concatenated vertically. In the feature-wise scheme, the feature maps for all five brain wave bands and a specific statistical feature were concatenated horizontally. In the whole trial scheme, the feature maps for all five brain wave bands and all three statistical features were concatenated in both directions. These concatenated feature maps then served as input for our dementia subtype classification model.

Outlier detection and rejection

To ensure data quality and minimize the impact of outliers, we implemented an outlier detection and rejection procedure. Initially, subject number three was excluded due to insufficient recording duration. Subsequently, for each group, we calculated the Mahalanobis distance for each trial based on the first two principal components derived from the statistical features across all electrode pairs, brain wave bands, and connectivity measures. Trials with Mahalanobis distances exceeding the 95th percentile of the chi-square distribution with one degree of freedom were considered outliers and rejected. Subjects with more than half of their trials rejected were also excluded from further analysis, resulting in the removal of nine subjects. To assess the impact of outlier rejection, we also report the results without outlier removal for comparison.

Classification model architecture

To classify dementia subtypes, we employed a CNN-based model tailored to process and analyze EEG feature maps[51,52]. Our architecture consisted of three 2-dimensional convolution stacks, followed by a global average pooling layer and a fully connected layer (Fig. 1).

Each convolutional stack consists of two 2-dimensional convolutional layers with a kernel size of 3, stride of 1, and a circular padding of 2. After each convolutional layer, we added a 2-dimensional dropout layer with a dropout rate of 0.25 and a 2-dimensional batch normalization layer to prevent overfitting. Moreover, we also applied an exponential linear unit (ELU) activation function following each normalization layer to introduce non-linearity[51,53]. The number of filters of the convolutional layer in each stack increased sequentially from 256 to 512 and finally to 1024. After each convolutional stack, a max pooling layer with a kernel size of 3 and a stride of 3 was used to reduce the spatial dimensions.

After convolutional stacks, a global average pooling layer was introduced to enforce correspondence between CNN features and predicted classes[54], then flattened into a one-dimensional array of size 1024. The fully connected stack comprised an artificial neural network with a single hidden layer with a size of 512. The hidden layer was followed by a sigmoid activation function and a dropout layer with a dropout rate of 0.5. Finally, the output layer consisted of three neurons (or two for pairwise classification) corresponding to the AD, FD, and HC groups. A SoftMax activation function was applied to obtain the probability of each class prediction. Lastly, the final predicted class was decided by the class with maximum probability.

Model training

To train and evaluate the classification model, we employed a stratified five-fold cross-validation scheme in a subject-wise manner, ensuring that all trials extracted from a subject were confined to a single fold. To address class imbalance within each fold, the Synthetic Minority Over-sampling Technique (SMOTE)[55] was applied to synthesize additional data on minority classes.

Hyperparameters were optimized using a grid search algorithm. The optimized hyperparameters include an AdamW optimizer[56] with a learning rate of 0.0001, a training batch size of 64 for AD/FD/HC classification task and 8 for binary classification tasks, a maximum training epoch of 1000, an early stopping regularization applied with the patience of 30, and a cross-entropy loss function. The learning curves of our best-performing models were displayed in Supplementary Figure S4-S7.

Model evaluation and xAI approach

The trained models were evaluated by their performance in predicting validation data. The performance metrics include accuracy and F1 score. Accuracy measures the percentage of correct predictions across all data. The F1 score is the harmonic mean of precision and sensitivity (or recall). Precision represents the percentage of correct predictions among all actual data in the given class, while sensitivity (or recall) is the percentage of correct predictions among all the data predicted as belonging to that class.

For binary classifications, the F1 score was calculated on the dementia group and FD group for AD/FD classification. For the multiclass classification, the macro-averaged F1 score was calculated by averaging the F1 score for individual classes.

Mean and SD of the accuracy and F1 score (or macro averaged F1 score) across all folds were reported for each study and input to provide an assessment of the model capability and stability in dementia subtypes classification.

The explainable artificial intelligence (xAI) approach involves interpreting deep learning models to understand how they make predictions. In this study, we visualize the CNN's intermediate features obtained after the global average pooling layer, predicting all trials, including outliers, using the t-distributed stochastic neighbor embedding (t-SNE) method[57]. This method reduces high-dimensional data to a lower dimension while preserving local similarities among data points. We fitted those intermediate features in two dimensions with a perplexity of 30. Trials with similar intermediate features will appear close to each other in the t-SNE visualization. For well-trained CNN models that can extract meaningful discriminative features for classification tasks, their t-SNE visualization should display well-separated clusters.

Data availability

The public dataset used in this study is accessible through the OpenNeuro Dataset ds004504 (https://openneuro.org/). The data generated during the current study and selected classification models are available at the author's GitHub repository (https://github.com/thawirasm-j/AlzNetV3).

Received: 26 November 2024; Accepted: 9 May 2025
Published online: 19 May 2025

References

1. American Psychiatric Association. Neurocognitive Disorders in Diagnostic and Statistical Manual of Mental Disorders, 5th Edn. 591–644. (American Psychiatric Association, 2013).
2. Hendriks, S. et al. Global prevalence of young-onset dementia: A systematic review and meta-analysis. *JAMA Neurol.* **78**, 1080–1090. https://doi.org/10.1001/jamaneurol.2021.2161 (2021).
3. Miltiadous, A. et al. A Dataset of scalp EEG recordings of alzheimer's disease, frontotemporal dementia and healthy subjects from routine EEG. *Data* **8** https://doi.org/10.3390/data8060095 (2023).
4. Shin, J. H. Dementia epidemiology fact sheet 2022. *Ann. Rehabil Med.* **46**, 53–59. https://doi.org/10.5535/arm.22027 (2022).
5. Bang, J., Spina, S. & Miller, B. L. Frontotemporal dementia. *Lancet* **386**, 1672–1682. https://doi.org/10.1016/S0140-6736(15)00461-4 (2015).
6. McMahon, P. M., Araki, S. S., Sandberg, E. A., Neumann, P. J. & Gazelle, G. S. Cost-effectiveness of PET in the diagnosis of alzheimer disease. *Radiology* **228**, 515–522. https://doi.org/10.1148/radiol.2282020915 (2003).
7. Khan, H. A. et al. The NMT scalp EEG dataset: An open-source annotated dataset of healthy and pathological EEG recordings for predictive modeling. *Front. Neurosci.* **15**, 755817. https://doi.org/10.3389/fnins.2021.755817 (2021).
8. Azuma, H. et al. An intervention to improve the interrater reliability of clinical EEG interpretations. *J. Neuropsychiatry Clin. Neurosci.* **57**, 485–489. https://doi.org/10.1046/j.1440-1819.2003.01152.x (2003).
9. Roy, Y. et al. Deep learning-based electroencephalography analysis: A systematic review. *J. Neural Eng.* **16** https://doi.org/10.1088/1741-2552/ab260c (2019).
10. Charupanit, K., Sen-Gupta, I., Lin, J. J. & Lopour, B. A. Detection of anomalous high-frequency events in human intracranial EEG. *Epilepsia Open.* **5**, 263–273. https://doi.org/10.1002/epi4.12397 (2020).
11. Zhao, S. et al. An interpretable model based on graph learning for diagnosis of Parkinson's disease with voice-related EEG. *Npj Digit. Med.* **7** https://doi.org/10.1038/s41746-023-00983-9 (2024).
12. Jafari, M. et al. Empowering precision medicine: AI-driven schizophrenia diagnosis via EEG signals: A comprehensive review from 2002–2023. *Appl. Intell.* **54**, 35–79. https://doi.org/10.1007/s10489-023-05155-6 (2024).
13. Ajra, Z., Xu, B., Dray, G., Montmain, J. & Perrey, S. Using shallow neural networks with functional connectivity from EEG signals for early diagnosis of Alzheimer's and frontotemporal dementia. *Front. Neurol.* **14** https://doi.org/10.3389/fneur.2023.1270405 (2023).
14. Miltiadous, A. et al. Alzheimer's disease and frontotemporal dementia: A robust classification method of EEG signals and a comparison of validation methods. *Diagnostics* **11**, 1437. https://doi.org/10.3390/diagnostics11081437 (2021).
15. Ge, Q., Lin, Z. C., Gao, Y. X. & Zhang, J. X. A robust discriminant framework based on functional biomarkers of EEG and its potential for diagnosis of Alzheimer's disease. *Healthcare* **8**, 476. https://doi.org/10.3390/healthcare8040476 (2020).
16. Cai, L. et al. Functional Integration and Segregation in Multiplex Brain Networks for Alzheimer's Disease. *Front. NeuroSci.* **14** https://doi.org/10.3389/fnins.2020.00051 (2020).

17. Prado, P. et al. Source space connectomics of neurodegeneration: One-metric approach does not fit all. *Neurobiol. Dis.* **179**, 106047. https://doi.org/10.1016/j.nbd.2023.106047 (2023).
18. Scherr, M. et al. Effective connectivity in the default mode network is distinctively disrupted in Alzheimer's disease—a simultaneous resting-state FDG-PET/fMRI study. *Hum. Brain. Mapp.* **42**, 4134–4143. https://doi.org/10.1002/hbm.24517 (2021).
19. Dennis, E. L. & Thompson, P. M. Functional brain connectivity using fMRI in aging and Alzheimer's disease. *Neuropsychol. Rev.* **24**, 49–62. https://doi.org/10.1007/s11065-014-9249-6 (2014).
20. Braak, H. & Braak, E. Neuropathological stageing of Alzheimer-related changes. *Acta Neuropathol.* **82**, 239–259. https://doi.org/10.1007/bf00308809 (1991).
21. Teipel, S. J. et al. Simultaneous assessment of electroencephalography microstates and resting state intrinsic networks in Alzheimer's disease and healthy aging. *Fronti. Neurol.* **12**. https://doi.org/10.3389/fneur.2021.637542 (2021).
22. Wirsich, J., Giraud, A. L. & Sadaghiani, S. Concurrent EEG- and fMRI-derived functional connectomes exhibit linked dynamics. *NeuroImage* **219** https://doi.org/10.1016/j.neuroimage.2020.116998 (2018).
23. Hata, M. et al. Functional connectivity assessed by resting state EEG correlates with cognitive decline of Alzheimer's disease—an eLORETA study. *Clin. Neurophysiol.* **127**, 1269–1278. https://doi.org/10.1016/j.clinph.2015.10.030 (2016).
24. Si, Y. et al. Differentiating between Alzheimer's disease and frontotemporal dementia based on the resting-state multilayer EEG network. *IEEE Trans. Neural Syst. Rehabil. Eng.* **31**, 4521–4527. https://doi.org/10.1109/TNSRE.2023.3329174 (2023).
25. Hafkemeijer, A. et al. Resting state functional connectivity differences between behavioral variant frontotemporal dementia and Alzheimer's disease. *Front. Hum. Neurosci.* **9** https://doi.org/10.3389/fnhum.2015.00474 (2015).
26. D'Amario, V., Srivastava, S., Sasaki, T. & Boix, X. The data efficiency of deep learning is degraded by unnecessary input dimensions. *Front. Comput. Neurosci.* **16** https://doi.org/10.3389/fncom.2022.760085 (2022).
27. Cao, J., Yang, L., Sarrigiannis, P. G., Blackburn, D. & Zhao, Y. Dementia classification using a graph neural network on imaging of effective brain connectivity. *Comput. Biol. Med.* **168**, 107701. https://doi.org/10.1016/j.compbiomed.2023.107701 (2024).
28. Barua, P. D., Tuncer, T., Baygin, M., Dogan, S. & Acharya, U. R. N-BodyPat: Investigation on the dementia and Alzheimer's disorder detection using EEG signals. *Knowl. Based Syst.* **304**, 112510. https://doi.org/10.1016/j.knosys.2024.112510 (2024).
29. Akbari, H. et al. Recognizing seizure using poincaré plot of EEG signals and graphical features in DWT domain. *Bratislava Med. Journal/Bratislavske Lekarske Listy* **124**, 12–24. https://doi.org/10.4149/BLL_2023_002 (2023).
30. Chen, Y., Wang, H., Zhang, D., Zhang, L. & Tao, L. Multi-feature fusion learning for Alzheimer's disease prediction using EEG signals in resting state. *Front. NeuroSci.* **17** https://doi.org/10.3389/fnins.2023.1272834 (2023).
31. Miltiadous, A., Gionanidis, E., Tzimourta, K. D., Giannakeas, N. & Tzallas, A. T. DICE-Net: A novel Convolution-Transformer architecture for alzheimer detection in EEG signals. *IEEE Access.* **11**, 71840–71858. https://doi.org/10.1109/ACCESS.2023.3294618 (2023).
32. Zheng, X. et al. Diagnosis of Alzheimer's disease via resting-state EEG: integration of spectrum, complexity, and synchronization signal features. *Front. Aging Neurosci.* **15** https://doi.org/10.3389/fnagi.2023.1288295 (2023).
33. Puri, D. V., Gawande, J. P., Rajput, J. L. & Nalbalwar, S. L. A novel optimal wavelet filter banks for automated diagnosis of Alzheimer's disease and mild cognitive impairment using electroencephalogram signals. *Decis. Analytics J.* **9**, 100336. https://doi.org/10.1016/j.dajour.2023.100336 (2023).
34. Zheng, H., Xiong, X., Zhang, X. & Multi-Threshold Recurrence Rate plot: A novel methodology for EEG analysis in Alzheimer's disease and frontotemporal dementia. *Brain Sci.* **14**, 565. https://doi.org/10.3390/brainsci14060565 (2024).
35. Rostamikia, M., Sarbaz, Y. & Makouei, S. EEG-based classification of Alzheimer's disease and frontotemporal dementia: A comprehensive analysis of discriminative features. *Cogn. Neurodyn.* **18**, 3447–3462. https://doi.org/10.1007/s11571-024-10152-7 (2024).
36. Ma, Y., Bland, J. K. S. & Fujinami, T. Classification of Alzheimer's disease and frontotemporal dementia using electroencephalography to quantify communication between electrode pairs. *Diagnostics* **14**, 2189. https://doi.org/10.3390/diagnostics14192189 (2024).
37. Yang, X., Fan, Z., Li, Z. & Zhou, J. Resting-state EEG microstate features for Alzheimer's disease classification. *PLOS ONE*. **19**, e0311958. https://doi.org/10.1371/journal.pone.0311958 (2024).
38. Puri, D. V. et al. Detection of Alzheimer's disease using spatiotemporal EEG analysis and low-complexity CNN. *IEEE Access* **12**, 113888–113897. https://doi.org/10.1109/ACCESS.2024.3435768 (2024). LEADNet.
39. Sadiq, M. T. et al. Exploiting pretrained CNN models for the development of an EEG-based robust BCI framework. *Comput. Biol. Med.* **143**, 105242. https://doi.org/10.1016/j.compbiomed.2022.105242 (2022).
40. Sadiq, M. T. et al. Toward the development of versatile brain–computer interfaces. *IEEE Trans. Artif. Intell.* **2**, 314–328. https://doi.org/10.1109/TAI.2021.3097307 (2021).
41. Alkhawaldeh, I. M., Albalkhi, I. & Naswhan, A. J. Challenges and limitations of synthetic minority oversampling techniques in machine learning. *World J. Methodol.* **13**, 373–378. https://doi.org/10.5662/wjm.v13.i5.373 (2023).
42. Kongwudhikunakorn, S. et al. A pilot study on visually stimulated cognitive tasks for EEG-Based dementia recognition. *IEEE Trans. Instrum. Meas.* **70**, 1–10. https://doi.org/10.1109/TIM.2021.3120131 (2021).
43. Ludwig, K. A. et al. Using a common average reference to improve cortical neuron recordings from microelectrode arrays. *J. Neurophysiol.* **101**, 1679–1689. https://doi.org/10.1152/jn.90989.2008 (2009).
44. Delorme, A. & Makeig, S. EEGLAB: an open source toolbox for analysis of single-trial EEG dynamics including independent component analysis. *J. Neurosci. Methods*. **134**, 9–21. https://doi.org/10.1016/j.jneumeth.2003.10.009 (2004).
45. Comon, P. Independent component analysis, A new concept? *Sig. Process.* **36**, 287–314. https://doi.org/10.1016/0165-1684(94)90029-9 (1994).
46. Pion-Tonachini, L., Kreutz-Delgado, K. & Makeig, S. ICLabel: An automated electroencephalographic independent component classifier, dataset, and website. *Neuroimage* **198**, 181–197. https://doi.org/10.1016/j.neuroimage.2019.05.026 (2019).
47. Castellanos, N. P., Makarov, V. A. & Recovering EEG brain signals: Artifact suppression with wavelet enhanced independent component analysis. *J. Neurosci. Methods* **158**, 300–312. https://doi.org/10.1016/j.jneumeth.2006.05.033 (2006).
48. Lachaux, J. P. et al. Studying single-trials of phase synchronous activity in the brain. *Int. J. Bifurc Chaos* **10**, 2429–2440. https://doi.org/10.1142/S0218127400001560 (2000).
49. Stam, C. J., Nolte, G. & Daffertshofer, A. Phase lag index: Assessment of functional connectivity from multi channel EEG and MEG with diminished bias from common sources. *Hum. Brain Mapp.* **28**, 1178–1193. https://doi.org/10.1002/hbm.20346 (2007).
50. Bruns, A., Eckhorn, R., Jokeit, H. & Ebner, A. Amplitude envelope correlation detects coupling among incoherent brain signals. *Neuroreport* **11**, 1509–1514 (2000).
51. Schirrmeister, R. T. et al. Deep learning with convolutional neural networks for EEG decoding and visualization. *Hum. Brain Mapp.* **38**, 5391–5420. https://doi.org/10.1002/hbm.23730 (2017).
52. Rakhmatulin, I., Dao, M. S., Nassibi, A. & Mandic, D. Exploring convolutional neural network architectures for EEG feature extraction. *Sensors* **24**, 877. https://doi.org/10.3390/s24030877 (2024).
53. Arı, E. & Taçgın, E. Input shape effect on classification performance of Raw EEG motor imagery signals with convolutional neural networks for use in Brain-Computer interfaces. *Brain Sci.* **13** https://doi.org/10.3390/brainsci13020240 (2023).
54. Lin, M., Chen, Q. & Yan, S. *Netw. Netw.* https://doi.org/10.48550/arXiv.1711.05101 (2013).
55. Chawla, N. V., Bowyer, K. W., Hall, L. O. & Kegelmeyer, W. P. SMOTE: Synthetic minority over-sampling technique. *J. Artif. Intell. Res.* **16**, 321–357. https://doi.org/10.1613/jair.953 (2002).
56. Loshchilov, I. & Hutter, F. Decoupled Weight Decay Regularization https://doi.org/10.48550/arXiv.1711.05101 (2019).
57. van der Maaten, L. & Hinton, G. Visualizing data using t-SNE. *J. Mach. Learn. Res.* **9**, 2579–2605 (2008).

Acknowledgements
This research was financially supported by Faculty of Medicine, Prince of Songkla University (MR PSU-673822-198/67-052-1).

Author contributions
T.J. and K.C. led and designed the project. T.J., P.L. and K.C. wrote and edited the main manuscript text. T.J., P.L. and K.C. prepared Figs. 1, 2, 3, 4 and 5. T.J. prepared Fig. 6, all supplementary figures and all tables. T.J., S.C. and K.R. collected the data and performed data cleaning. Formal analysis was performed by T.J. and S.C. All authors reviewed the manuscript.

Competing interests
The authors declare no competing interests.

Additional information
Supplementary Information The online version contains supplementary material available at https://doi.org/10.1038/s41598-025-02018-7.

Correspondence and requests for materials should be addressed to K.C.

Reprints and permissions information is available at www.nature.com/reprints.

Publisher's note Springer Nature remains neutral with regard to jurisdictional claims in published maps and institutional affiliations.